IEEE Access
Multidisciplinary | Rapid Review | Open Access Journal

Received June 15, 2021, accepted June 28, 2021, date of publication July 1, 2021, date of current version July 14, 2021.

Digital Object Identifier 10.1109/ACCESS.2021.3094028

Triple-Band Concurrent Reconfigurable Matching Network

JESÚS DE MINGO, PEDRO LUIS CARRO, PALOMA GARCÍA-DÚCAR, AND ANTONIO VALDOVINOS

Department of Electronics Engineering and Communications, University of Zaragoza, 50018 Zaragoza, Spain

Corresponding author: Jesús de Mingo (mingo@unizar.es)

This work was supported in part by the Ministerio de Ciencia e Innovacion (MICCIN) through the Fondo Europeo de Desarrollo Regional (FEDER) under Project RTI2018-095684-B-I00, and in part by the Diputacion General de Aragon (DGA) under Grant T31_17R.

This work did not involve human subjects or animals in its research.

ABSTRACT Reconfigurable Matching Networks (RMN) have found a wide range of applications, such as antenna impedance matching (Antenna Tuning Units -ATU-), the design of reconfigurable power amplifiers, applications in Magnetic Resonance Imaging (MRI), adjustable low noise amplifier design, etc. In this paper, we propose the experimental design and verification of a reconfigurable impedance synthesis network that can simultaneously work in three different bands and is completely independent so that the impedance variations in a frequency band are approximately transparent to the rest. The variable elements used in this paper are varactors. To verify its operation, it is applied to a process of matching a laser modulator in three different frequency bands for C-RAN (Cloud Radio Access Networks) applications. Experimental results demonstrate, as expected, that losses may depend on the state in which they are driven. Consequently, a state that can guarantee a good match could also imply greater losses, leading to a certain trade-off. The application of genetic algorithms in this context points out that it may be convenient to optimize the insertion losses of the complete chain instead of the return losses.

INDEX TERMS Multiband reconfigurable matching network (RMN), reconfigurable devices, load-pull.

I. INTRODUCTION

Radio frequency front ends for current and future radio communication systems are expected to be reconfigurable as far as possible [1]. New reconfigurable architectures are intended to be fully multiband and concurrent. There are multiple references related to ''Reconfigurable Matching Networks'' (RMNs) for different applications in a single band, explaining the simple process of adapting transmit and receive antenna impedances [2], [3] as well as the search for improvement in transmission efficiency, both from the broadband, multiband or reconfigurable frequency band point of view. Examples of power amplifiers based on Doherty technology [4], Envelope Tracking (ET) [5], Dynamic Load Modulation [6] or in other applications such as Tunable Diplexer [7] or the design of reconfigurable transmitters [8] using Tunable Matching Networks (TMNs) (also known as reconfigurable matching networks (RMN) [20]) for reconfigurable amplifiers or in applications like MRI [16] have been extensively studied and designed for multiple purposes.

The article focuses on the design and assembly of a multiband RMN system which operates concurrently so that changes in the RMN in one band do not affect, as far as possible, to another band (bands work as independent RMNs). This assembly allows various applications, from simultaneous multiband system adaptation, to the design of power stages with tunable loads to first, second and third harmonic.

This paper is organized as follows. Section II presents the design of RMNs for three different bands using varactors. Section III describes the RMN topology for the three concurrent simultaneous bands. Section IV proposes the test set-up and results corresponding to different prototype measurements. Section V includes possible applications and Section VI concludes this paper.

II. RMN BY BAND DESIGN

In order to show the process steps, the design of three RMNs centered on three LTE bands, 826 MHz

The associate editor coordinating the review of this manuscript and approving it for publication was Mario Donato Marino.

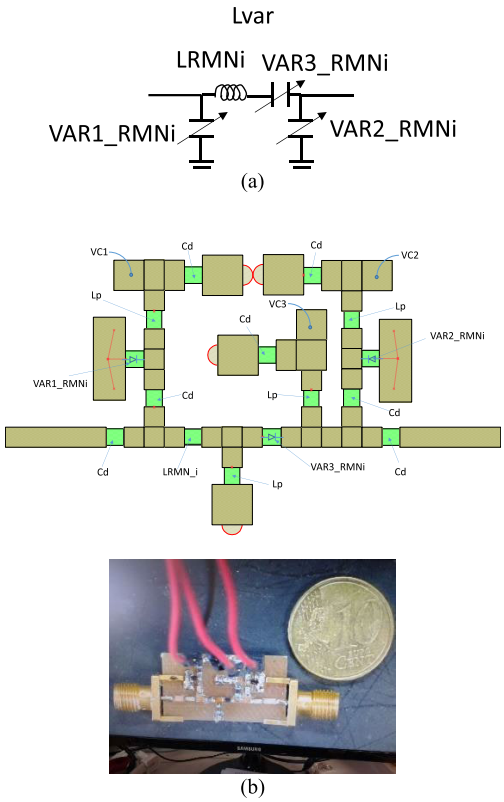

FIGURE 1. a) Schematic of the proposed ∏ topology. b) Layout and assembly generated with AWR including polarization networks for control signals and decoupling capacitors.

(791-862 MHz), 1795 MHZ (1710-1880 MHz) and 2595 MHz (2500-2690 MHz) is proposed without loss of generality. As a starting point, a ∏ topology [2], [8] is selected. In addition, a variable inductor is built by means of a fixed value element together with a series varactor [9], [18], [19]. Fig. 1.a shows the proposed topology and Fig. 1.b the layout.

Before choosing the suitable varactors, a study of the range of variation in the values of the capacitors and inductors presented in Fig.1 (a) was carried out in order to synthesize a large number of impedances for every band in the proposed network. Thus, for each frequency bands, the choice of different varactors and inductors available on the market was used.

The DC bias circuitry including DC and RF blocks are included in the simulation model and a definitive prototype is showed in Fig 1(b).

The control signal biasing networks and decoupling capacitors with values Lp = 270nH, Cd = 100pF, are the same in all reconfigurable networks whereas the selected varactors, as well as the LRMNi value, change for each frequency band. The reason is that we seek to maximize the number of synthesizable points by the network in every band. Table 1 shows the references of the varactors and values of the inductors selected for each frequency band. The substrate is FR4 with a thickness of 1.54 mm.

Fig. 2 shows the models and the variation of the capacity presented by the varactors for different biasing voltages and

TABLE 1. Values of the components associated with each RMN by bands.

RMN1 (791-862 MHz)	RMN2 (1710-1880 MHz)	RMN3 (2500-2690 MHz)
VAR1_RMN1:VARACTOR1	VAR1_RMN2:VARACTOR2	VAR1_RMN3:VARACTOR3
VAR2_RMN1:VARACTOR2	VAR2_RMN2:VARACTOR2	VAR2_RMN3:VARACTOR3
VAR3_RMN1:VARACTOR1	VAR2_RMN2:VARACTOR2	VAR3_RMN3:VARACTOR3
LRMN_1= 18 nH	LRMN_2: 6.8 nH	LRMN_3: 3.6 nH

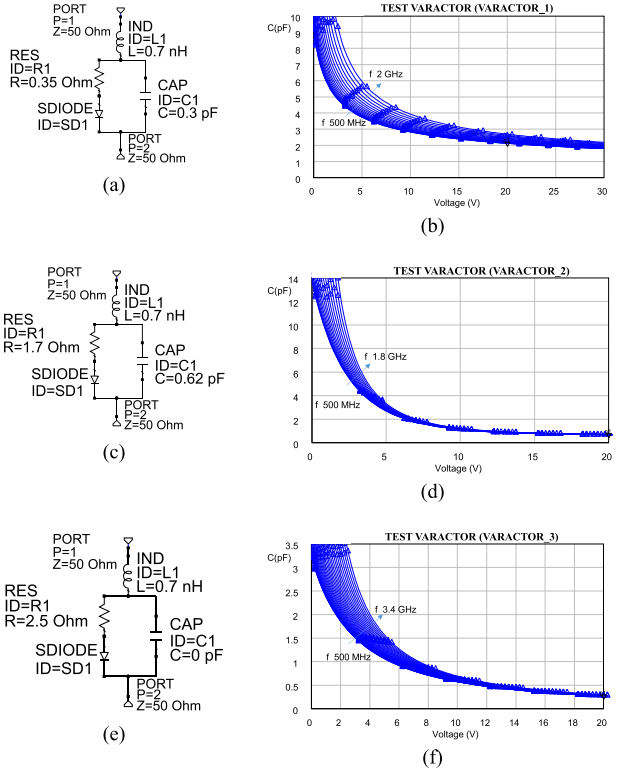

FIGURE 2. (a) and (b) Model and capacity variation as a function of voltage and frequency, respectively, of the VARACTOR1. (c) and (d) of the VARACTOR2. (e) and (f) of the VARACTOR3.

frequencies. Varactor modelling is achieved with the aid of the data provided by the manufacturer.

Fig. 3 shows the results obtained for each RMN, both simulated and measured, for every proposed frequency band. The voltage steps in the control signals presented in the measurements are increased with respect to those computed by simulation to reduce the measurement time, which results in a less concentrated point cloud on the Smith Chart. The comparison between the simulations and measurements for different frequency bands shows certain differences. As frequency increases, the edges of the Smith chart are not covered because of the effect of losses. Besides, it must be pointed out that simulations neglect real effects such as the soldering of the components or the vias hole to ground.

III. CONCURRENT RMNS TOPOLOGY AND FREQUENCY BAND ISOLATION

Each RMN designed and presented in the previous section for every band is part of the core of the complete system of the concurrent multiband RMN.

The assembly presented in Fig. 4 precisely seeks independent operation and decreases the effects that some subnetworks have respect to others. In the figure, RMNs (i = 1 . . . 3) are those previously designed and the MBF_i_in/out blocks (Multiband Filter Band i) are the filters at the input and the output of the RMNi respectively. These are identically arranged as mirror symmetry with respect to the vertical axis, and must have high impedance at the input and output for the rest of the bands and null insertion losses in their band of interest. This is shown with the reflection coefficients in each access port of each branch according to the frequency band to be processed in Fig. 4. In the same figure, each branch can be interpreted as a concatenation of filters at the input and output of the RMN studied in the previous section (MBF_i_in + RMNi + MBF_i_out), and the RMNi corresponding to the i-th band. From the serial cascade of the networks for each branch/band, a two port network SNi (when i denotes the i-th band) can be defined and the S parameters for the SNi network can be obtained. The analytical expressions are presented in eqs. (1-4), as shown at the bottom of this page [10], where i = 1,2,3 corresponds to the 3 selected frequency bands.

The MBFs (MultiBand Filters) should be totally transparent to the band where they have to work and should present an open circuit behaviour for the remaining bands to lead to a correct and ideal system operation. Therefore, the S parameters of the network formed by the input and output filters in each of the i-th branches must comply Eq (5-7). For the branch 1, corresponding to the branch that acts on frequency band 1:

$$S^{MBF\_1\_in/out}\,(Band\_1) = \begin{bmatrix} 0 & 1 \\ 1 & 0 \end{bmatrix} \tag{5}$$

$$S^{MBF\_1\_in/out}\,(Band\_2) = \begin{bmatrix} +1 & 0 \\ 0 & +1 \end{bmatrix} \tag{6}$$

$$S^{MBF\_1\_in/out}\,(Band\_3) = \begin{bmatrix} +1 & 0 \\ 0 & +1 \end{bmatrix} \tag{7}$$

In this way, SN1, denoting the concatenation of the (MBF_1_in + RMN1 + MBF_1_out) in the branch 1, for the different bands, applying Eq. (5-7) to Eq. (1-4) would present the following S parameters:

$$SN1\,(Band\_1) = \begin{bmatrix} S_{11}^{RMN1}\,(Band\_1) & S_{12}^{RMN1}\,(Band\_1) \\ S_{21}^{RMN1}\,(Band\_1) & S_{22}^{RMN1}\,(Band\_1) \end{bmatrix} \tag{8}$$

$$SN1\,(Band\_2) = \begin{bmatrix} +1 & 0 \\ 0 & +1 \end{bmatrix} \tag{9}$$

$$SN1\,(Band\_3) = \begin{bmatrix} +1 & 0 \\ 0 & +1 \end{bmatrix} \tag{10}$$

$$SNi_{11} = S_{11}^{MBF\_i\_in} + \frac{S_{12}^{MBF\_i\_in} \cdot S_{21}^{MBF\_i\_in} \cdot S_{11}^{RMNi}}{1 - S_{22}^{MBF\_i\_in} \cdot S_{11}^{RMNi}} + \frac{\dfrac{S_{12}^{MBF\_i\_in} \cdot S_{12}^{RMNi}}{1 - S_{22}^{MBF\_i\_in} \cdot S_{11}^{RMNi}} \cdot \dfrac{S_{21}^{MBF\_i\_in} \cdot S_{21}^{RMNi}}{1 - S_{22}^{MBF\_i\_in} \cdot S_{11}^{RMNi}} \cdot S_{11}^{MBF\_i\_out}}{1 - \left(S_{22}^{RMNi} + \dfrac{S_{21}^{RMNi} \cdot S_{12}^{RMNi} \cdot S_{22}^{MBF\_i\_in}}{1 - S_{11}^{RMNi} \cdot S_{22}^{MBF\_i\_in}} \right) \cdot S_{11}^{MBF\_i\_out}} \tag{1}$$

$$SNi_{12} = \frac{\dfrac{S_{12}^{MBF\_i\_in} \cdot S_{12}^{RMNi}}{1 - S_{22}^{MBF\_i\_in} \cdot S_{11}^{RMNi}} \cdot S_{12}^{MBF\_i\_out}}{1 - \left(S_{22}^{RMNi} + \dfrac{S_{21}^{RMNi} \cdot S_{12}^{RMNi} \cdot S_{22}^{MBF\_i\_in}}{1 - S_{11}^{RMNi} \cdot S_{22}^{MBF\_i\_in}} \right) \cdot S_{11}^{MBF\_i\_out}} \tag{2}$$

$$SNi_{21} = \frac{\dfrac{S_{21}^{MBF\_i\_in} \cdot S_{21}^{RMNi}}{1 - S_{22}^{MBF\_i\_in} \cdot S_{11}^{RMNi}} \cdot S_{21}^{MBF\_i\_out}}{1 - \left(S_{22}^{RMNi} + \dfrac{S_{21}^{RMNi} \cdot S_{12}^{RMNi} \cdot S_{22}^{MBF\_i\_in}}{1 - S_{11}^{RMNi} \cdot S_{22}^{MBF\_i\_in}} \right) \cdot S_{11}^{MBF\_i\_out}} \tag{3}$$

$$SNi_{22} = S_{22}^{MBF\_i\_out} + \frac{S_{21}^{MBF\_i\_out} \cdot S_{12}^{MBF\_i\_out} \cdot \left(S_{22}^{RMNi} + \dfrac{S_{21}^{RMNi} \cdot S_{12}^{RMNi} \cdot S_{22}^{MBF\_i\_in}}{1 - S_{11}^{RMNi} \cdot S_{22}^{MBF\_i\_in}} \right)}{1 - \left(S_{22}^{RMNi} + \dfrac{S_{21}^{RMNi} \cdot S_{12}^{RMNi} \cdot S_{22}^{MBF\_i\_in}}{1 - S_{11}^{RMNi} \cdot S_{22}^{MBF\_i\_in}} \right) \cdot S_{11}^{MBF\_i\_out}} \tag{4}$$

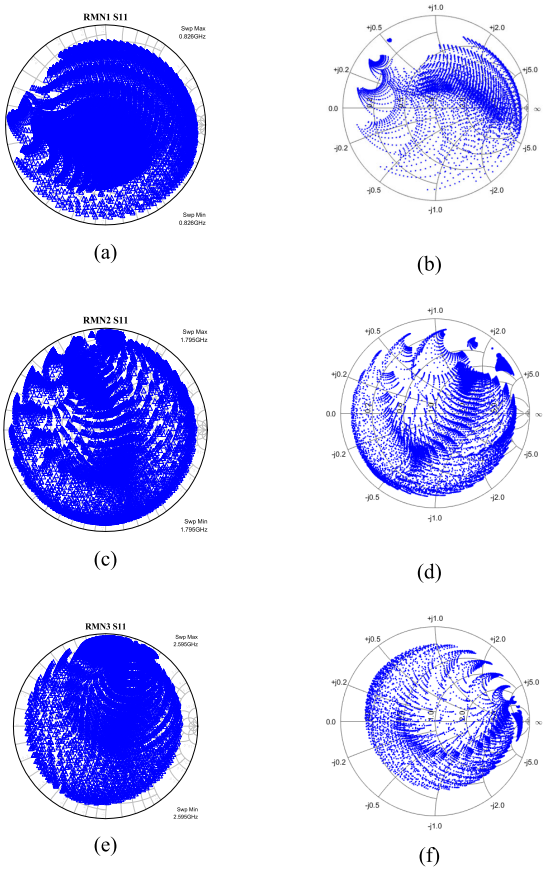

FIGURE 3. (a) and (b) S11 at 826 MHz simulated and measured respectively for RMN1. (c) and (d) S11 at 1,795 GHz for RMN2 and (e) and (f) S11 at 2,595 GHz for RMN3.

Therefore, for the frequency band 1, the branch 1 would present the S parameter of the RMN1 and for the rest of the bands it would present an open circuit at its input and output.

Accordingly, the input and output MBFs band 2 branch responses at the different frequencies fulfill:

$$S^{MBF\_2\_in/out}\,(Band\_2) = \begin{bmatrix} 0 & 1 \\ 1 & 0 \end{bmatrix} \tag{11}$$

$$S^{MBF\_2\_in/out}\,(Band\_1) = \begin{bmatrix} +1 & 0 \\ 0 & +1 \end{bmatrix} \tag{12}$$

$$S^{MBF\_2\_in/out}\,(Band\_3) = \begin{bmatrix} +1 & 0 \\ 0 & +1 \end{bmatrix} \tag{13}$$

With the following S parameters, once Eq. (11-12) has been applied in (1-4) for the concatenated network SN2:

$$SN2\,(Band\_2) = \begin{bmatrix} S_{11}^{RMN2}\,(Band\_2) & S_{12}^{RMN2}\,(Band\_2) \\ S_{21}^{RMN2}\,(Band\_2) & S_{22}^{RMN1}\,(Band\_2) \end{bmatrix} \tag{14}$$

$$SN2\,(Band\_1) = \begin{bmatrix} +1 & 0 \\ 0 & +1 \end{bmatrix} \tag{15}$$

$$SN2\,(Band\_3) = \begin{bmatrix} +1 & 0 \\ 0 & +1 \end{bmatrix} \tag{16}$$

Finally, in the third band, the subnetwork scattering parameters are imposed to be:

$$S^{MBF\_3\_in/out}\,(Band\_3) = \begin{bmatrix} 0 & 1 \\ 1 & 0 \end{bmatrix} \tag{17}$$

$$S^{MBF\_3\_in/out}\,(Band\_1) = \begin{bmatrix} +1 & 0 \\ 0 & +1 \end{bmatrix} \tag{18}$$

$$S^{MBF\_3\_in/out}\,(Band\_2) = \begin{bmatrix} +1 & 0 \\ 0 & +1 \end{bmatrix} \tag{19}$$

And the S parameters for the third branch will be SN3:

$$SN3\,(Band\_3) = \begin{bmatrix} S_{11}^{RMN3}\,(Band\_3) & S_{12}^{RMN3}\,(Band\_3) \\ S_{21}^{RMN3}\,(Band\_3) & S_{22}^{RMN3}\,(Band\_3) \end{bmatrix} \tag{20}$$

$$SN3\,(Band\_1) = \begin{bmatrix} +1 & 0 \\ 0 & +1 \end{bmatrix} \tag{21}$$

$$SN3\,(Band\_2) = \begin{bmatrix} +1 & 0 \\ 0 & +1 \end{bmatrix} \tag{22}$$

The scheme of Fig. 5 helps to understand the selective operation in the different bands and describes the parallel subnetwork connection. We will work with their equivalent admittance parameters, since we have three ports in parallel, to properly figure out how the final circuit works.

Let be the matrix [YT] and [ST] the whole network admittance parameters and S parameters, respectively. As the network assembly is connected in parallel, they are the direct sum of the admittance parameters of each subnetwork:

$$[YT] = [YN1] + [YN2] + [YN3] \tag{23}$$

According to the previous described operation, the total network will present the following individual frequency behaviour. For example, in the case of the first frequency band the networks in branches 2 and 3 will present an open circuit at their input and output, verifying (24),

$$\left[\,YN2\,(Band\_1)\,\right] = \left[\,YN3\,(Band\_1)\,\right] = [0] \tag{24}$$

$$[YT\,(Band\_1)] = \left[\,YN1\,(Band\_1)\,\right] \tag{25}$$

Therefore, applying (23) the S parameters of whole network will be

$$\begin{aligned} ST\,(Band\_1) &= SN1\,(Band\_1) \\ &= \begin{bmatrix} S_{11}^{RMN1}\,(Band\_1) & S_{12}^{RMN1}\,(Band\_1) \\ S_{21}^{RMN1}\,(Band\_1) & S_{22}^{RMN1}\,(Band\_1) \end{bmatrix} \end{aligned} \tag{26}$$

Applying the same idea to the other frequency bands,

$$\begin{aligned} ST\,(Band\_2) &= SN2\,(Band\_2) \\ &= \begin{bmatrix} S_{11}^{RMN2}\,(Band\_2) & S_{12}^{RMN2}\,(Band\_2) \\ S_{21}^{RMN2}\,(Band\_2) & S_{22}^{RMN1}\,(Band\_2) \end{bmatrix} \end{aligned} \tag{27}$$

$$\begin{aligned} ST\,(Band\_3) &= SN3\,(Band\_3) \\ &= \begin{bmatrix} S_{11}^{RMN3}\,(Band\_3) & S_{12}^{RMN3}\,(Band\_3) \\ S_{21}^{RMN3}\,(Band\_3) & S_{22}^{RMN3}\,(Band\_3) \end{bmatrix} \end{aligned} \tag{28}$$

Thus and ideally, frequency band isolation is proved and the tuning in one subnetwork will not impact on the matching process in the other subnetworks.

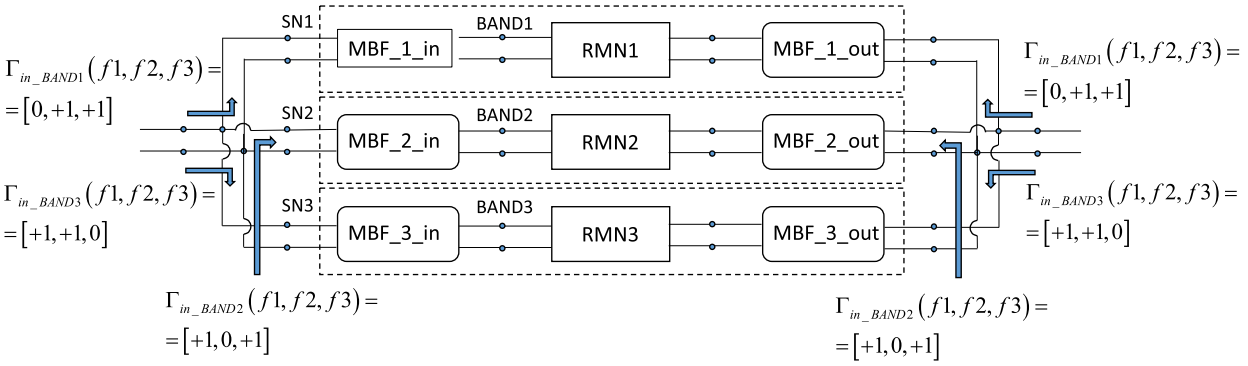

FIGURE 4. Proposed topology for the concurrent multiband reconfigurable network.

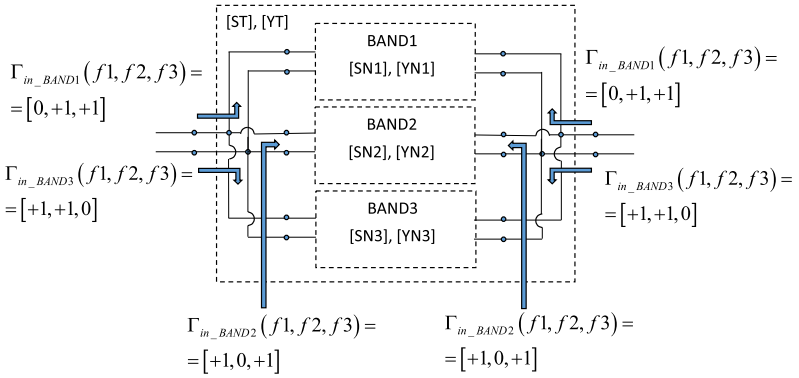

FIGURE 5. Proposed topology for the concurrent multiband reconfigurable network and its equivalence in total admittance parameters.

TABLE 2. Proposal of the MBF_1 topology and its behaviour according to the different frequencies.

MBF_1 f1<f2<f3	Approximated Frequency Response	Target Ideal Frequency Response
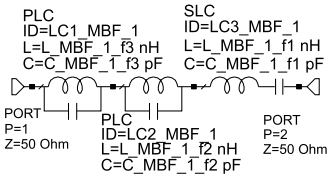	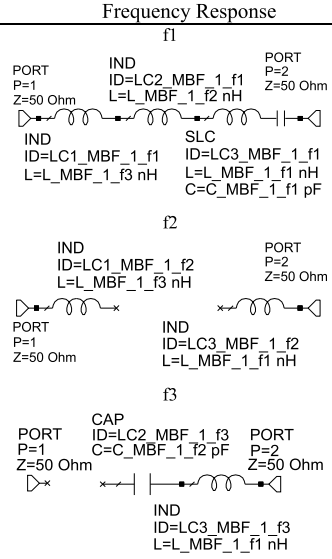	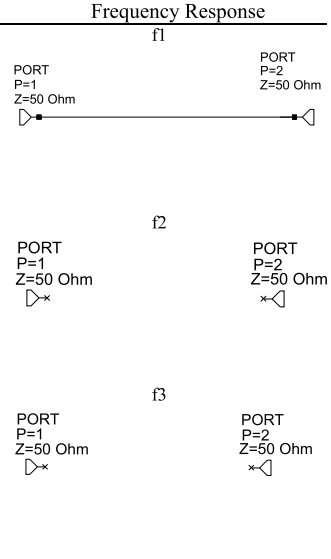

IV. EXPERIMENTAL TEST-BED AND MEASUREMENT RESULTS

This section aims at describing the operation of the total network proposal. First of all, it is important to define the reference connection planes of the three subnetworks corresponding to the different frequency bands of interest. Secondly, two design conditions (C1 and C2) should be met by each MBF:

-C1: an open circuit should be reached at the input ports in every branch in the two frequency bands which are not the target frequency band where the considered subnetwork operates.

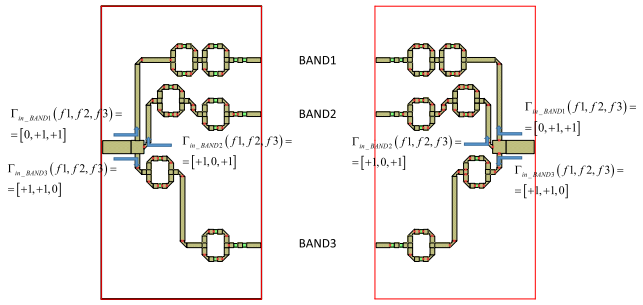

FIGURE 6. Layout of the proposed assembly for the band filtering system.

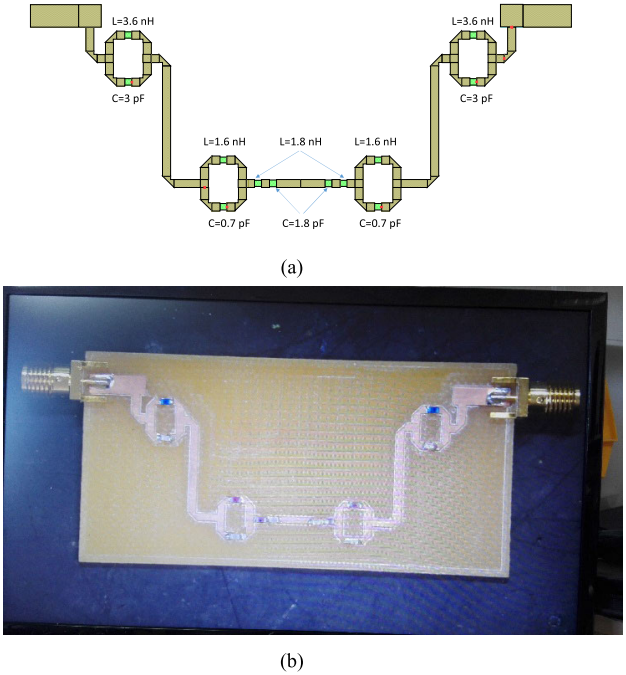

(a)

(b)

FIGURE 7. Prototype to verify the operation of the filter branches for band 3 in a back to back assembly (a) Layout; (b) prototype.

-C2: suitable impedance matching in the target band where each subnetwork works must be achieved.

If the MBF filter is developed with the aid of resonant LC parallel immittances, C1 is accomplished outside the target frequency because they show open circuit behaviour at the remaining frequency bands (a high impedance is created). In addition, a series resonator in the target frequency band has to be included. Table 2 shows the practical MBF implementation in the case of the MBF_1.

Specifically, The MBF_1 influence on different bands is analyzed. At low frequency (f1) the resonant tank circuits at the frequencies f2 and f3 respectively approximately behave like an inductance. At frequency f2 the circuit tank to f2 resonates presenting high impedance, while the tank to f1 will have an inductive behaviour and the series resonator to f1 as well. Finally, at the high frequency f3, the tank circuit at f3 will present high impedance, from the tank circuit at f2, which behaves in this case as the capacitor, and from the series resonator, the inductor value. A similar reasoning can be performed on the different bands.

TABLE 3. Values of the selected components for the resonators in each band.

MBF	TANK CIRCUIT 1	TANK CIRCUIT 2	SERIE RESONATOR
MBF_1:	L=3.6 nH, C=0.3 pF	L=3.9 nH, C=0.6 pF	L=8.7 nH, C=47 pF
MBF_2:	L=3.6 nH, C=3 pF	L=1.8 nH, C=0.3 pF	L=4.7 nH, C=2.4 pF
MBF_3:	L=3.6 nH, C=3 pF	L=1.6 nH, C=0.7 pF	L=1.8 nH, C=1.8 pF

The resonance frequencies corresponding to the MBF_1 are, (29), as shown at the bottom of the next page.

$$\omega_2 \approx \frac{1}{\sqrt{(\text{L\_MBF\_1\_f2}) \cdot (\text{C\_MBF\_1\_f2})}} \tag{30}$$

$$\omega_3 \approx \frac{1}{\sqrt{(\text{L\_MBF\_1\_f3}) \cdot (\text{C\_MBF\_1\_f3})}} \tag{31}$$

Following a similar procedure for MBF_2, the serial resonator should resonate at frequency f2 and the resonators parallel at frequencies f1 and f3, and for MBF_3 the serial resonator should resonate at frequency f3 and the resonators parallel at frequencies f1 and f2.

As far as the element interconnection is concerned, microstrip transmission lines, connection points between tracks, etc., must be taken into account in the design and assembly process. Fig. 6 shows this implementation step showing the interconnection between elements and branches.

The physical microstrip line lengths must be adjusted to achieve the interconnection between the inputs and outputs of the RMNs. They are computed to get the following reflection coefficients at the access ports of MBF networks as a function of frequencies

$$\Gamma_{in\_BAND1}\,(f1, f\,2, f3) = [0, +1, +1] \tag{32}$$

$$\Gamma_{in\_BAND2}\,(f1, f\,2, f3) = [+1, 0, +1] \tag{33}$$

$$\Gamma_{in\_BAND3}\,(f1, f\,2, f3) = [+1, +1, 0] \tag{34}$$

Table 3 summarizes the values obtained after the simulation process including microstrip lines and interconnections.

To verify the correct operation, the assembly of the MBF_3 of BAND 3 is measured in a back to back connection as shown in Fig. 7.

Fig. 8 shows initial measurements with real values. The differences between the computed magnitudes which come out from simulations, and the feasible lumped real values requires some final tuning so that each subnetwork response resembles the ideal frequency behaviour.

This final tuning process concerns not only the values of the matching network itself, but also takes into account SMA-PCB connectors and vias hole electrical models [17]. Connectors have been modelled as a low pass lumped pi circuit using the following values: a 0.261 pF capacitor to input, 0.872 nH serial inductor and 0.244 pF capacitor to output, which come from a standard extraction procedure.

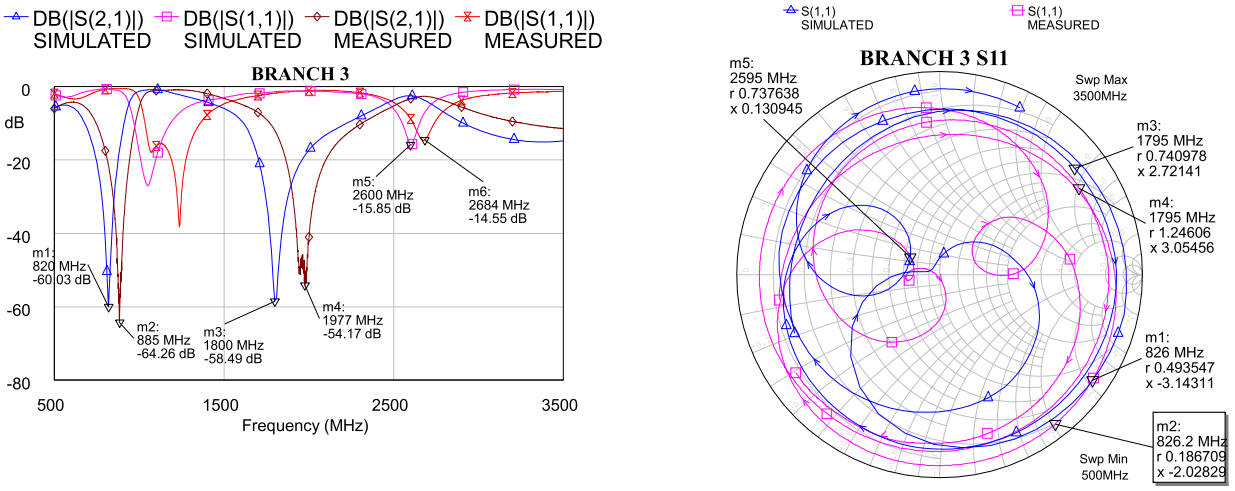

FIGURE 8. Comparison between measured and simulations of the back to back assembly for the branch for band 3.

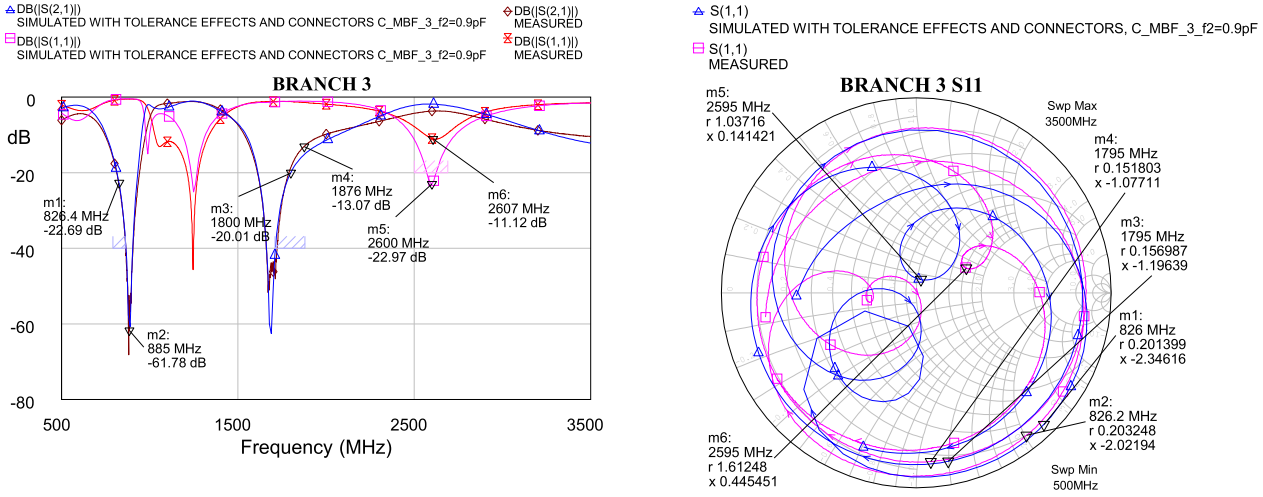

FIGURE 9. Comparison between measured and simulated after final tuning for band 3.

Fig. 9 shows measured and simulated results with the final tuning.

The reflection coefficient in the interconnection planes in the different bands are estimated using a deembeding which is performed on the prototype measurements. The method moves the reference plane to the previously specified point. Thus,

$$\Gamma_{in\_BAND3}\,(f1, f2, f3) = [+1, +1, 0]\,.$$

Fig. 10 presents the obtained result, where the proximity to the open circuit is observed at the frequencies f1 and f2.

The final test-bed implementation (Fig. 11) comprises not only the filters, but also the RMNs which are located at every branch. As a result, the triple-band concurrent design is concluded.

Fig. 12 presents the results corresponding to the synthesizable points in the Smith chart (coverage region) through the S22 parameter. This is carried out by means of a varactor bias sweep (in 1 volt. steps). Three varactors (those in every subnetwork) vary and the remaining are kept at their maximum voltage. Hence they are set to their lowest capacitive value. The coverage region in the target and concurrent bands is represented with the complete varactor sweep. Therefore, the isolation effect between bands, whose coverage region should ideally be as small as possible (i.e. one point), is identified. Furthermore, the losses included by the filter networks

$$\omega_1 \approx \frac{1}{\sqrt{(\text{L\_MBF\_1\_f3} + \text{L\_MBF\_1\_f2+L\_MBF\_1\_f1}) \cdot \text{C\_MBF\_1\_f1}}} \tag{29}$$

(components, transmission lines…) decrease the coverage area.

V. RADIO-OVER-FIBER ARCHITECTURE APPLICATION

This section presents an application example for C-RAN (Cloud Radio Access Network) technology [11]–[13]. The MultiBand Reconfigurable Matching Networks (MB-RMNs) will be used to match the input impedance of a laser modulator, in the three bands mentioned above. The laser modulator will be connected to a 10 km of optic fiber to connect it to a laser detector.

Fig. 13 shows the proposal and assembly where a vector network analyser is used for evaluating the performance of the complete chain. The power supplies which act on the control signals of the network varactors are controlled by means of a computer and the measurements obtained by the vector network analyser are captured.

To evaluate the performance of the system, measurements are made with and without the MB-RMNs at the input of the laser modulator. Two optimization search algorithms are then carried out with the MB-RMNs applying genetic algorithms. Firstly, the optimization focuses on the S11 parameter which is minimized in each band separately. The optimization problem is 9-dimensional (three variables for each band), taking into account the isolation, reducing the computation time because the variables are independent for each band. Thus, the search space is remarkably reduced. The proposed cost function is to find the minimum of parameter S11, but other cost functions could be applied, such as maximizing S21 parameter as it will be proposed later.

Fig. 14 (a) and (b) shows the results obtained for parameters S11 and S21 of the global assembly with and without the MB-RMN respectively. It shows a significant improvement in return losses, of more than 35 dB in 826 MHz, more than 25 dB in 1795 MHz, and more than 50 dB in 2595 MHz. However, insertion loss improvements of the order of 5 dB are achieved in the 826 MHz frequency, decreasing around 1.5 dB in 1795 MHZ and 4 dB in 2595 MHz. The latter cases are due to the losses introduced by the networks.

The best input impedance matching states do not have to agree with the best states of minimum insertion losses. Although there is a clear relationship, the fact that the dissipative losses may vary depending on the states proposed to the network [13], [14], [22], [23] makes that both conditions could be achieved in different configurations. To verify this statement, an optimization process is also carried out by applying genetic algorithms, but using as an objective function the insertion losses and thus, we seek to maximize S21. Thanks to the band isolation the computational efforts are decreased throughout a search space size reduction as in the case of the optimization of the S11.

Fig. 15 (a) and (b) shows the S21 and S11 parameter performance of the global assembly with and without the MB-RMN, respectively, using parameter S21 as a cost function. An improvement of 5 dB in the frequency of 826 MHz is observed in this case for S21, similar to the previous

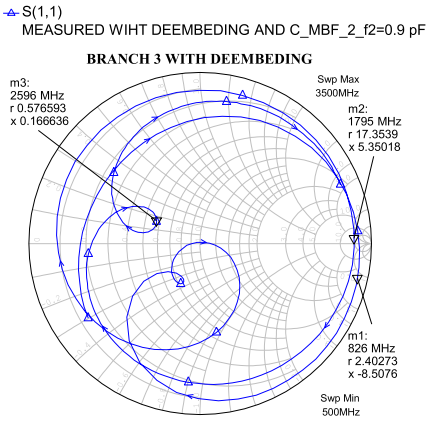

FIGURE 10. Result obtained from the prototype measurement of the branch 3 after fine tuning and reference plane deembeeding.

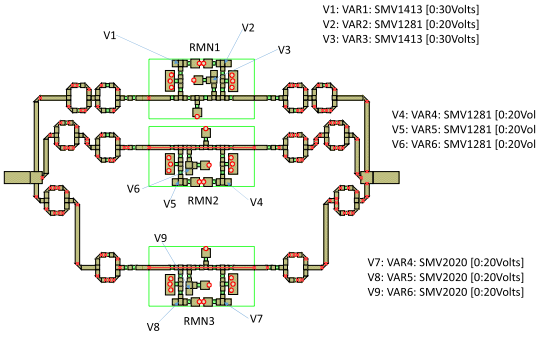

(a)

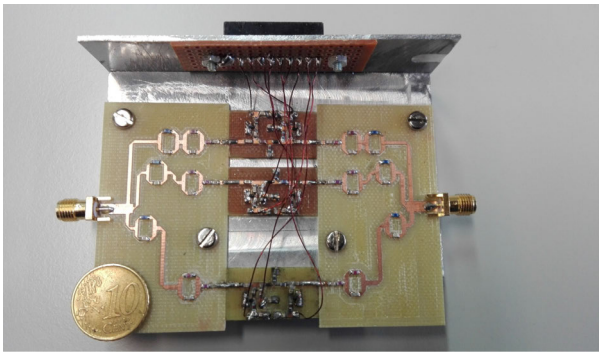

(b)

FIGURE 11. Complete assembly of multiband RMNs. (a) Layout; (b) prototype.

situation, a worsening of 0.7 dB (vs. 1.5 dB worsening shown in Fig 14) at 1795 MHz and 0.38 dB (vs. 4 dB worsening shown in Fig 14) at 2595 MHz. Regarding return losses, in this case, it is observed, in comparison with previous situation, an improvement in return losses around 20 dB (vs. 35 dB shown in Fig 14) in 826 MHz, around 18 dB (vs. 25 dB shown in Fig 14) in 1795 MHz, and around 10 dB (vs. 50 dB shown in Fig 14) in 2595 MHz.

Different losses introduced by the network in these new states, lower than those previously obtained, justify

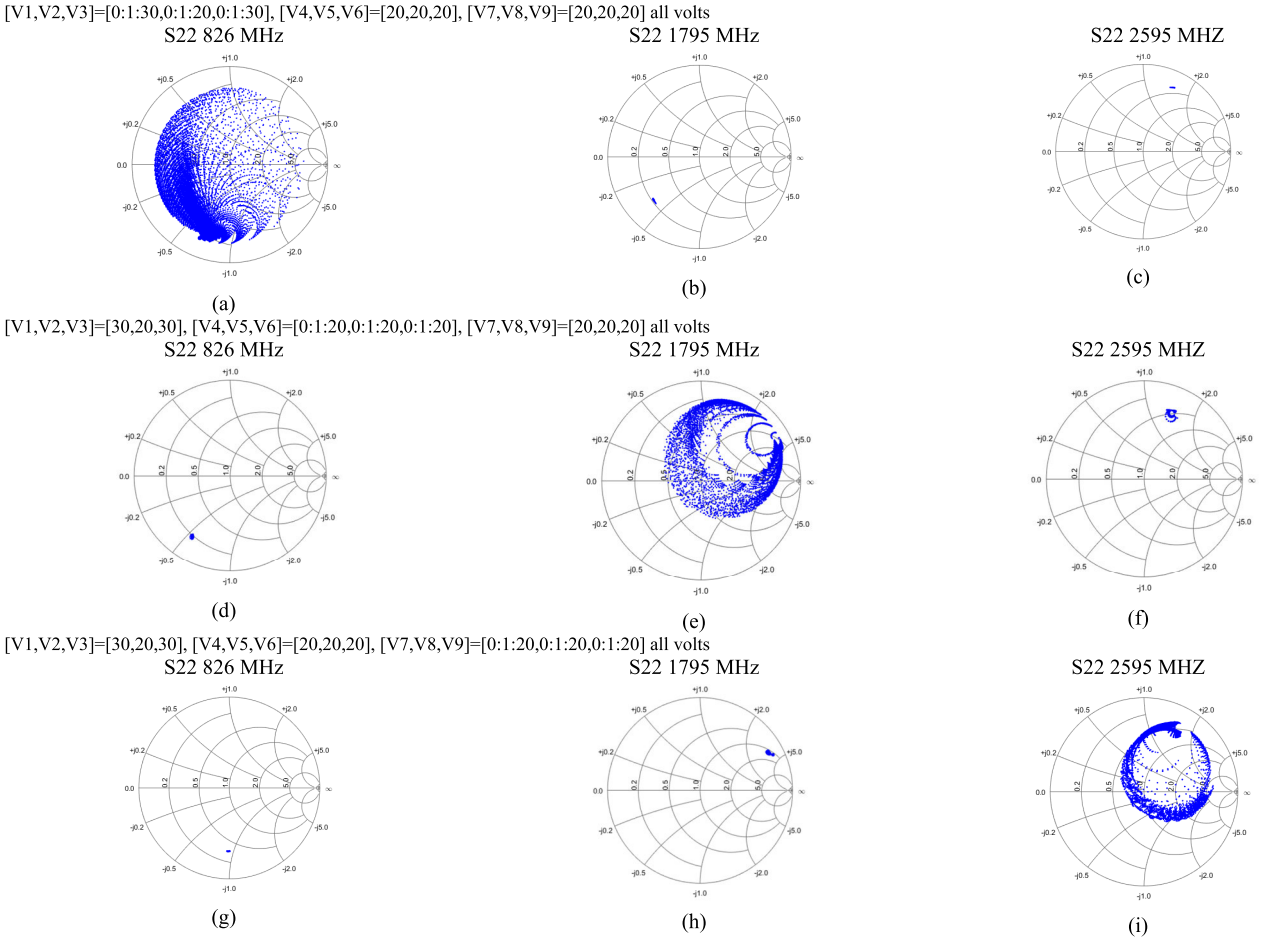

FIGURE 12. Measurements coverage and isolation by bands according to the variations of the varactors of each one of the RMNs. (a), (b), (c) point cloud in the Smith chart synthesizable with the variables V1, V2, V3 of the RMN1 and variation in the rest of the bands. (d), (e), (f) point cloud in the Smith chart synthesizable with the variables V4, V5, V6 of the RMN2 and variation in the rest of the bands. (g), (h), (i) point cloud in the Smith chart synthesizable with the variables V7, V8, V9 of the RMN3 and variation in the rest of the bands.

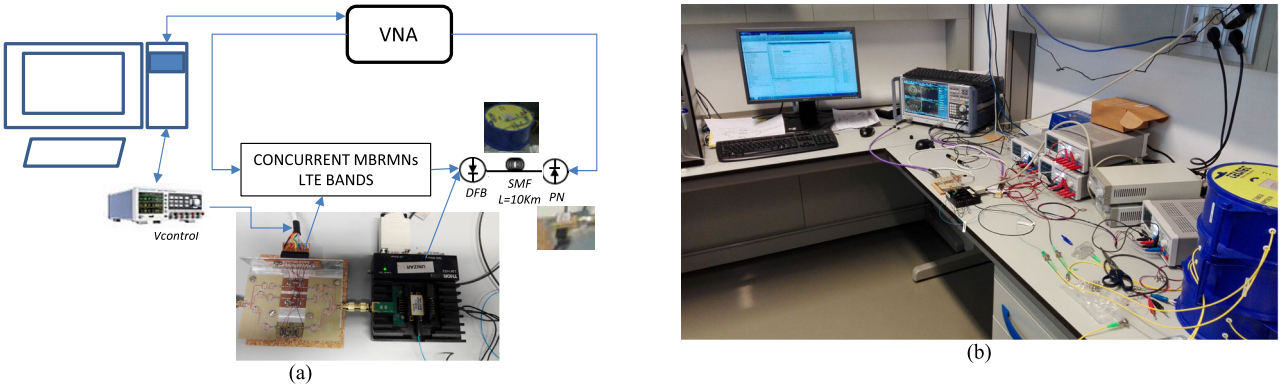

FIGURE 13. Assembly of the measurement system for C-RAN application.

these new results. In contrast to return loss optimization solutions and despite the fact that substantial improvements are also obtained, they are not as great as in the previous situation, where the cost function to be optimized was precisely the return losses for each of the bands. The use of a low cost substrate and the losses added by varactors, inductors and capacitors mean that the expected improvements in insertion losses are not as good as desired.

VI. CONCLUSION

The design process of a multi-band Reconfigurable Matching Network (RMN), called Multiband Reconfigurable Matching Network (MB-RMN), has been presented, with the ability to

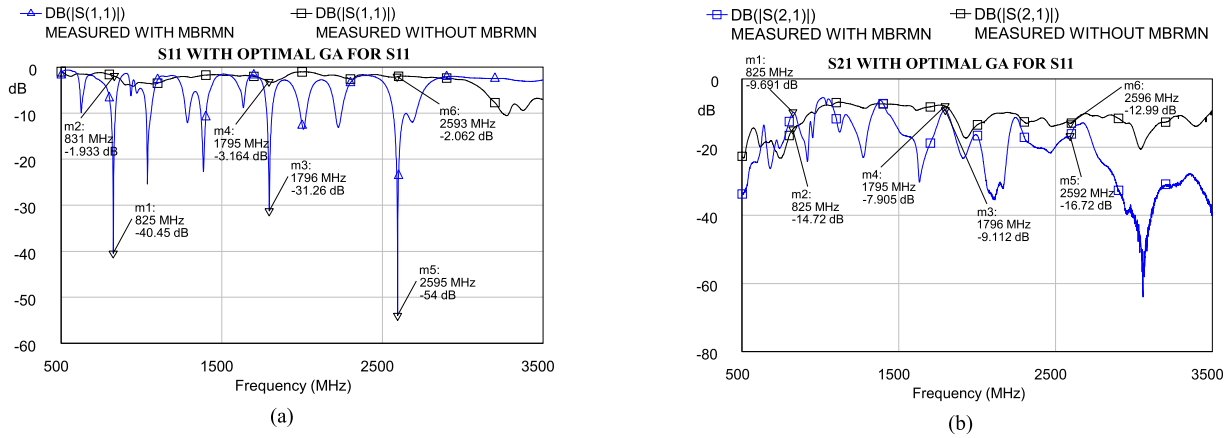

FIGURE 14. Comparative results with and without MBRMNs with the S11 optimization application using genetic algorithms. a) regarding the S11 parameters measured with and without MBRMNs. b) regarding the S21 parameters measured with and without MBRMNs.

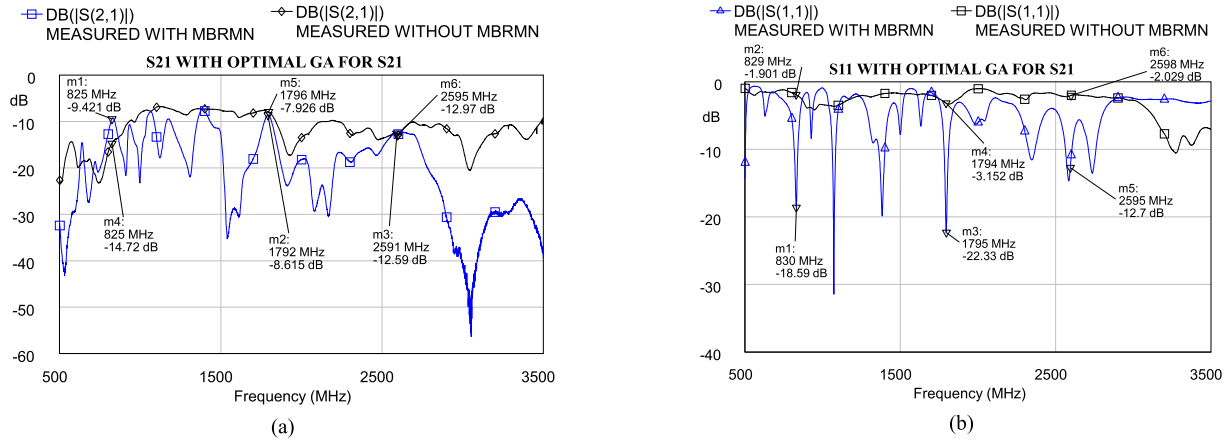

FIGURE 15. Comparative results with and without MBRMNs with the S21 optimization application using genetic algorithms. a) regarding the S21 parameters measured with and without MBRMNs. b) regarding S11 parameters measured with and without MBRMNs.

concurrently work on different frequency bands, that is, the operation of the network in each band without the variations made in one band affecting the rest of the bands. Its operation has been presented in a possible C-RAN application (Cloud Radio Access Network) where the use of three LTE bands is proposed simultaneously. Different triple-band state optimizations yield to different optimal solutions, showing the impact of losses on Smith Chart coverage and return and insertion loss performances.

ACKNOWLEDGMENT

The authors would like to thank to José Luis Pérez Yecora for the collaboration in the assembly of the prototypes.

REFERENCES

[1] H. Okazaki, T. Furuta, K. Kawai, Y. Takagi, A. Fukuda, and S. Narahashi, "Reconfigurable RF circuits for future multi-mode multi-band mobile terminals," in *Proc. Int. Symp. Electromagn. Theory*, Hiroshima, Japan, May 2013, pp. 432–435.

[2] J. deMingo, A. Valdovinos, A. Crespo, D. Navarro, and P. Garcia, "An RF electronically controlled impedance tuning network design and its application to an antenna input impedance automatic matching system," *IEEE Trans. Microw. Theory Techn.*, vol. 52, no. 2, pp. 489–497, Feb. 2004.

[3] C. Sanchez-Perez, J. De Mingo, P. Garcia-Ducar, and P. L. Carro, "Signal-to-noise maximization in DVB-H receivers using reconfigurable matching networks," *IEEE Trans. Consum. Electron.*, vol. 56, no. 3, pp. 1349–1355, Aug. 2010.

[4] D. Gustafsson, C. M. Andersson, and C. Fager, "A modified Doherty power amplifier with extended bandwidth and reconfigurable efficiency," *IEEE Trans. Microw. Theory Techn.*, vol. 61, no. 1, pp. 533–542, Jan. 2013.

[5] S. Park, J.-L. Woo, M.-S. Jeon, U. Kim, and Y. Kwon, "Broadband CMOS stacked power amplifier using reconfigurable interstage network for envelope tracking application," in *Proc. IEEE Radio Freq. Integr. Circuits Symp.*, Jun. 2014, pp. 145–148.

[6] C. Sanchez-Perez, M. Ozen, C. M. Andersson, D. Kuylenstierna, N. Rorsman, and C. Fager, "Optimized design of a dual-band power amplifier with SiC varactor-based dynamic load modulation," *IEEE Trans. Microw. Theory Techn.*, vol. 63, no. 8, pp. 2579–2588, Aug. 2015.

[7] C.-H. Ko and G. M. Rebeiz, "A 1.4–2.3-GHz tunable diplexer based on reconfigurable matching networks," *IEEE Trans. Microw. Theory Techn.*, vol. 63, no. 5, pp. 1595–1602, May 2015.

[8] C. Hoarau, N. Corrao, J.-D. Arnould, P. Ferrari, and P. Xavier, "Complete design and measurement methodology for a tunable RF impedance-matching network," *IEEE Trans. Microw. Theory Techn.*, vol. 56, no. 11, pp. 2620–2627, Nov. 2008.

[9] M. Tsuji, T. Nishikawa, K. Wakino, and T. Kitazawa, "Bi-directionally fed phased-array antenna downsized with variable impedance phase shifter for ISM band," *IEEE Trans. Microw. Theory Techn.*, vol. 54, no. 7, pp. 2962–2969, Jul. 2006.

[10] K. C. Gupta, R. Garg, and R. Chadha, *Computer-Aided Design of Microwave Circuits*. Washington, DC, USA: Hartech House, 1981.
[11] A. Checko *et al.*, "Clud RAN for mobile networks—A technology overwiew," *IEEE Commun. Surveys Tuts.*, vol. 17, no. 1, pp. 405–426. [Online]. Available: https://www.researchgate.net/publication/273706693_Cloud_RAN_for_Mobile_Networks-A_Technology_Overview and https://groups.google.com/group/gnuradio-usrp-ch/attach/d1a4191c0206bcdd/CRAN_white_paper_v1%2014.pdf?part=0.1
[12] D. Lee, H. Seo, B. Clerckx, E. Hardouin, D. Mazzarese, S. Nagata, and K. Sayana, "Coordinated multipoint transmission and reception in LTE-advanced: Deployment scenarios and operational challenges," *IEEE Commun. Mag.*, vol. 50, no. 2, pp. 148–155, Feb. 2012.
[13] A. J. Cooper, "Fibre/radio for the provision of cordless/mobile telephony services in the access network," *Electron. Lett.*, vol. 26, no. 24, pp. 2054–2056, 1990.
[14] C. Sanchez, J. de Mingo, L. Saenz, P. Garcia, P. L. Carro, and A. Valdovinos, "Performance evaluation of an automatic impedance synthesizer based on RF switches," in *Proc. VTC Spring IEEE 69th Veh. Technol. Conf.*, Apr. 2009, pp. 1–5.
[15] C. Sanchez-Perez, C. M. Andersson, K. Buisman, D. Kuylenstierna, N. Rorsman, and C. Fager, "Design and large-signal characterization of high-power varactor-based impedance tuners," *IEEE Trans. Microw. Theory Techn.*, vol. 66, no. 4, pp. 1744–1753, Apr. 2018.
[16] S. M. Sohn, L. DelaBarre, A. Gopinath, and J. T. Vaughan, "Design of an electrically automated RF transceiver head coil in MRI," *IEEE Trans. Biomed. Circuits Syst.*, vol. 9, no. 5, pp. 725–732, Oct. 2015.
[17] Y. Zhao, S. Hemour, T. Liu, and K. Wu, "Nonuniformly distributed electronic impedance synthesizer," *IEEE Trans. Microw. Theory Techn.*, vol. 66, no. 11, pp. 4883–4897, Nov. 2018.
[18] Q. Gu, J. R. De Luis, A. S. Morris, and J. Hilbert, "An analytical algorithm for pi-network impedance tuners," *IEEE Trans. Circuits Syst. I, Reg. Papers*, vol. 58, no. 12, pp. 2894–2905, Dec. 2011.
[19] C.-I. Lee and W.-C. Lin, "A novel p-i-n inductor for tunable wideband matching network application," *IEEE Trans. Electron Devices*, vol. 60, no. 8, pp. 2611–2618, Aug. 2013.
[20] G. Lee, J. Jung, and J.-I. Song, "A multiband power amplifier with a reconfigurable output-matching network for 10-MHz BW LTE mobile phone applications," *IEEE Trans. Circuits Syst. II, Exp. Briefs*, vol. 62, no. 6, pp. 558–562, Jun. 2015.
[21] J.-R. Perez-Cisneros, J. de Mingo, P. L. Carro, P. Garcia-Ducar, C. Mateo, A. Valdovinos, and C. Sanchez-Perez, "2-D optimization methodology for reconfigurable transmitters by tunable matching networks," *IEEE Trans. Circuits Syst. II, Exp. Briefs*, vol. 64, no. 11, pp. 1277–1281, Nov. 2017.
[22] C. Sanchez-Perez, J. Mingo, P. Garcia-Ducar, and P. Carro, "Performance improvement of mobile DVB-H terminals using a reconfigurable impedance tuning network," *IEEE Trans. Consum. Electron.*, vol. 55, no. 4, pp. 1875–1882, Nov. 2009.
[23] N. J. Smith, C.-C. Chen, and J. L. Volakis, "An improved topology for adaptive agile impedance tuners," *IEEE Antennas Wireless Propag. Lett.*, vol. 12, pp. 92–95, 2013.

JESÚS DE MINGO was born in Barcelona, Spain, in 1965. He received the Ingeniero de Telecomunicación degree from the Universidad Politécnica de Cataluña (UPC), Barcelona, in 1991, and the Doctor Ingeniero de Telecomunicación degree from the Universidad de Zaragoza, in 1997. From 1991 to 1992, he joined the Antenas Microondas y Radar Group, Departamento de Teoría de la Señal y Comunicaciones. From 1992 to 1993, he was employed at Mier Comunicaciones S.A., where he worked in the solid state power amplifier design. He has been an Assistant Professor, since 1993, an Associate Professor, since 2001, and a Full Professor with the Departamento de Ingeniería Electrónica y Comunicaciones, Universidad de Zaragoza, since 2017. He is also a member of the Aragon Institute of Engineering Research (I3A). His research interests include the area of linearization techniques of power amplifiers, power amplifier design, and mobile antenna systems.

PEDRO LUIS CARRO was born in Zaragoza, Spain, in 1979. He received the M.S. degree in telecommunication engineering and the Ph.D. degree from the University of Zaragoza, in 2003 and 2009, respectively. In 2002, he carried out his master thesis on antennas for mobile communications with the Department of GSM and Antenna Products, Ericsson Microwave Systems, A.B., Göteborg (Sweden). From 2002 to 2004, he was employed at RYMSA S.A., where he worked with the Space and Defense Department, as an Electrical Engineer, and involved in the design of antennas and passive microwave devices for satellite communication systems. From 2004 to 2005, he worked with the Research and Development Department, TELNET Redes Inteligentes, as a RF Engineer, involved in radio over fiber systems. In 2005, he joined the Department of Electronics Engineering and Communications, University of Zaragoza, as an Assistant Professor. His research interests include the area of mobile antenna systems, passive microwave devices, and power amplifiers.

PALOMA GARCÍA-DÚCAR was born in Zaragoza, Spain, in 1972. She received the degree in telecommunications engineering and the Ph.D. degree from the University of Zaragoza, Spain, in 1996 and 2005, respectively. In 1995, she was employed at Teltronic S.A.U., where she worked in the Research and Development Department, involved in the design of radio communication systems (mobile equipment and base station), until 2002. From 1997 to 2001, she has collaborated in several projects with the Communication Technologies Group, Department of Electronics Engineering and Communications, University of Zaragoza. In 2002, she joined the Centro Politécnico Superior, University of Zaragoza, where she is currently an Assistant Professor. She is also involved as a Researcher with the Aragon Institute of Engineering Research (I3A). Her research interests include the area of linearization techniques of power amplifiers, and signal processing techniques for radio communication systems.

ANTONIO VALDOVINOS received the degree in telecommunications engineering and the Ph.D. degree from the Universitat Politècnica de Catalunya (UPC), Spain, in 1990 and 1994, respectively. He was with UPC and the University of Zaragoza, where he has been a Full Professor, since 2003. His research interests include 5G/4G technologies, heterogeneous communication networks, and mission-critical communication networks, with emphasis on transmission techniques, radio resource management and quality of service, mobility management, and planning and dimensioning of mobile networks.